Journal of Molecular Liquids 397 (2024) 124093

Contents lists available at ScienceDirect

Journal of Molecular Liquids

journal homepage: www.elsevier.com/locate/molliq

Ionogels based on protic ionic liquid - lithium salt mixtures

J.J. Parajó [a,b,1], P. Vallet [a,1], M. Villanueva [a], O. Cabeza [c], F. Fernández-Carretero [d], A. García Luis [d], M.E. Di Pietro [e], A. Mele [e], F. Castiglione [e], J. Salgado [a,*], L.M. Varela [a,*]

[a] NAFOMAT Group, Departamentos de Física Aplicada y Física de Partículas, Instituto de Materiales (iMATUS), Universidade de Santiago de Compostela, 15782 Santiago de Compostela. Spain
[b] CIQUP, Institute of Molecular Sciences (IMS) - Departamento de Química e Bioquímica, Faculdade de Ciências da Universidade do Porto, Rua do Campo Alegre, P-4169-007 Porto, Portugal
[c] Mesturas Group, Physics and Earth Sciences Department, Universidade da Coruña, 15071 A Coruña, Spain
[d] Tecnalia Research and Innovation, Parque Científico y Tecnológico de Bizkaia, C/Geldo, Edif. 700 Derio-Bizkaia 48160, Spain
[e] Politecnico di Milano, Departmentof Chemistry, Materials and Chemical Engineering "G.Natta" Piazza L. da Vinci32, 20133 Milano, Italy

ARTICLE INFO

Keywords:
Ionogels
Ionic liquid–metal salt mixtures
Liquid range
Ionic conductivity

ABSTRACT

The effect of the addition of lithium nitrate on the liquid range and electrical conductivity of mixtures of a protic ionic liquid, ethylammonium nitrate (EAN) with $LiNO_3$ is reported in this work. Moreover, changes in these properties upon confinement in silica-based matrices are also analysed and related to variations on the microstructure of the mixtures. Our results show that gelation of the mixtures induces amorphous behaviour in all the samples, but no significant changes in the thermal stability are detected. However, important differences on the electrical conductivity of the liquid and gel states of the mixtures were observed. While this magnitude decreases with the addition of salt in the liquid samples for all the temperatures it increases at low concentrations of $LiNO_3$ up to a maximum in the gelled samples with the lowest concentration of added salt (0.1 mol of salt by kg of EAN). High resolution magic angle spinning (HRMAS) NMR shows that the addition of lithium nitrate increases the mobility (both rotational and translational motion) of the cation EA^+ within the ionogel and the diffusion of the cation provides evidence of the presence of two different populations of the same molecules experiencing two distinct apparent diffusion coefficients (bi-exponential decay of magnetization in diffusion NMR experiments), while it is mono-exponential in the pure ionic liquid. The Li^+ cation is shown to display a higher mobility (both rotational and translational motion) in the ionogel than in the neat ionic liquid. The frustration of the formation of solvation complexes due to the confinement is suspected to be behind this behaviour.

1. Introduction

Energy transition is one of the major topics in the current agenda of our societies. Then, currently electrochemical energy storage plays a crucial role towards the decarbonisation of the electricity sector by improving the integration and exploitation of renewable energy sources, with an outstanding role for the Li-ion batteries.

The design of the novel electrolytes for commercially available energy storage devices is a major scientific challenge nowadays, current lithium-ion batteries are mainly based on organic carbonates with added lithium salts [1], offering good electrical conductivities, despite as organic solvents are volatile and highly flammable, limiting the safety of these devices. During the last years smart new electrolytes and ionogels based on mixtures of ionic liquids (ILs) with inorganic salts have been proposed with regards to their good electrical properties, good thermal and chemical stabilities and low toxicity [2–4].

ILs are defined as salts formed by asymmetric ions with very low lattice energies that allow them to be liquid in a large temperature range, including room temperature. Their important properties include their extremely high electrochemical and thermal stabilities, their non-flammability and undetectable vapour pressure, moreover high ionic conductivity, which can be tuned by means of the addition of electrochemically stable organic molecular cosolvents [5,6]. These characteristics make them optimal candidates for energy applications [7], as, for example, electrolytes for next generation high-voltage batteries, advanced supercapacitors or last generation ILs/fuel cells [8,9].

* Corresponding authors.
E-mail addresses: j.salgado.carballo@usc.es (J. Salgado), luismiguel.varela@usc.es (L.M. Varela).
[1] Contributed equally to this work.

https://doi.org/10.1016/j.molliq.2024.124093
Received 11 January 2023; Received in revised form 15 January 2024; Accepted 17 January 2024
Available online 22 January 2024

Table 1
Chemical compounds used in this work.

NameMolecular mass ($g \cdot mol^{-1}$)	Abbreviation CAS number	Chemical structure	Purity Supplier
Ethylammonium Nitrate 108.0965	EAN 22113–86-6	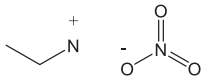	>0.97[a] Iolitec
Lithium Nitrate 68.946	$LiNO_3$ 7790–69-4	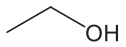	>0.999[b] Merck
Tetraethyl orthosilicate 208.33	TEOS 78–10-4	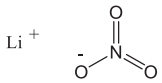	>0.999[b] Sigma Aldrich
Formic acid	FA 78–10-4	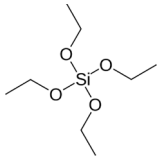	>0.98 Scharlau
Ethanol	EtOH 78–10-4	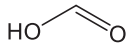	>0.99 PanReac

[a] Determined by NMR.
[b] Indicated by provider.

Ethylammonium nitrate (EAN) is the first synthesized IL, therefore, one of the most studied, and is currently used in a wide number of applications as electrically conductive solvent in electrochemistry [10] or as protein crystallization agent [11]. Mixtures of this IL with different solvents as water or other organic solvents have also been considered as electrolytes for energy storage devices (fuel cells or supercapacitors), both experimental [12,13] or theoretical and simulation studies [14,15], since the solvation of the ions of the EAN by the solvent leads to a reduction of electrostatic forces and H-bonds, increasing conductivity due to increased charge carriers [16]. Furthermore, EAN + nitrate salts (mainly lithium nitrate) mixtures are of particular interest in the electrochemical field. This system has been the subject of study in recent years and our group has contributed several reference works in the field. These works, that lead to the formulation of the nanostructured solvation paradigm, concluded that EAN essentially preserves its structure after salt addition, lithium cations are inserting in the charged domains, avoiding the apolar part of the structure and lithium is solvated forming tetrahedral complexes [2,17,18]. Other authors also reported important observations, for example Filippov et al [16] suggest that the mean number of anions near the cation amino group increases with the lithium salt concentration, and lithium ions accumulate in the structure of aggregates formed by hydrophobic chains of the IL cation. They also indicate that temperature and salt concentration play a fundamental role in the degree of dissociation of ion aggregates and thus in conductivity behaviour, finding that 6 mol % is a critical concentration.

However, liquid electrolytes present important problems of safety and performance [7]. The development of 4th generation batteries strongly relies on the availability of solid-state (or semi-solid) electrolytes of high enough electrical conductivity [19]. The design of safe and non-flammable novel electrolytes, compatible with different electrodes in electrochemical devices is currently one of the major topics of both fundamental and applied research in the field of electrochemical energy storage [20]. Recent studies suggest the possibility of micro or nano confining ILs and their mixtures with inorganic salts in gel matrices, achieving high mechanical stability while preserving liquid state ionic conductivities [21,22]. Specifically, mechanically rigid preparations made by nanoconfinement of ILs in a gel matrix (ionogels) have shown to provide optimal quasi-solid electrolytes [21], since they combine the mechanical rigidity expected from solid electrolytes, with liquid-state conductivities. Organosilica matrix forming materials have been used for the encapsulation of IL-based electrolytes in electrochemical devices, [23,24] although the behaviour of some key properties of the gel phase such as ionic conductivity are still scarcely known. ILs and their mixtures with cosolvents encapsulated in a solid-like hybrid gel matrix emerge as optimal candidates for the replacement of currently employed organic electrolytes, since the effect of the confinement on the structure and transport properties of IL/metal salt mixtures must be properly assessed.

Studies addressing the effects of EAN confinement are scarce. Li et al. [25] underlined improvements in both mechanical response and optical properties of EAN ionogels against hydrogels. Filippov et al. [26] found an increase in the diffusion of the ions of EAN after the confinement between thin glass plates separated a few microns with regards to the bulk IL, suggesting changes in the structure of the EAN before and after the confinement, that can be mainly attributed to the presence and modification of the hydrogen-bonding networks [27]. Up to our knowledge, studies about ionogels of mixtures of EAN and lithium salts have not been reported in the literature.

In this work, we propose a complete study of the structure, thermal behaviour, electrical conductivity, and lithium transport of ionogels of the protic IL ethyl ammonium nitrate (EAN), doped with lithium nitrate salt. This study is an extension of previous works of our groups that collect results of several properties of liquid samples of EAN + nitrate salts mixtures [24,28].

The structure of the paper is as follows: after this introduction, the experimental details are reported and, in the following section, we include the discussion of our results. Finally, we summarize the conclusions of the paper.

2. Materials and methods

2.1. Chemicals

Ethylammonium nitrate (EAN) was purchased from IOLITEC.

Solutions of EAN with $LiNO_3$ salt, provided by Merck, in three different concentrations, in the molality range from 0.1 mol·kg^{-1} up to the saturation limit (2 mol·kg^{-1}) [28], were prepared. Table 1 shows the identification, chemical structure, purity and origin of the chemicals used for this work. Water content of EAN and $LiNO_3$ salt have been checked by Karl-Fischer titration.

The different solutions of the salts were prepared by mixing both components with the help of an ultrasound bath during 24 to 48 h. Before the mixture preparation, EAN sample was dried under vacuum for a minimum of 48 h. Residual amount of water was tested with a Karl Fischer titrator, and this content was shown to be less than 100 ppm.

2.2. Gelation routes

Two different routes have been used in this work to prepare the silica based gels of the mixtures of EAN with Li salt:

1. Formic acid route: Gelation process has been performed by slightly modifying the methodology of Negre *et al.* [23]. A solid like ionogel-based electrolyte was synthetized using TEOS (TetraEthylOrthoSilicate) under acidic conditions (Formic Acid, FA) in a volumetric ratio TEOS:FA 1:2. The reactants were mixed under moderate stirring (300 rpm) at 40 °C during 18 min. Finally, 4 ml of liquid mixture of IL + Li salt were added, previously prepared following the methodology described in Ref. [28]. The resulting solution was stored in sealed containers and kept at room temperature until complete gelation achieved and aged for approximately one week.
2. Ethanol route: This method is an adaptation of a methodology previously reported [19,29]. A mixture of 3 ml of ethanol + 0.428 ml of TEOS + 1 ml of EAN-salt mixture was firstly prepared. These mixtures were stirred for 1 h, and then and before gelation, transferred to appropriate vials for 1–2 h. The vials were maintained at 40 °C in an oven until full gelation (4 days) to evaporate the excess of ethanol.

2.3. Experimental section

2.3.1. IR spectroscopy

ATR-FTIR spectra were recorded with a FTIR VARIAN model 670-IR equipped with a pike GladiATR with diamond crystal and single reflection in 400–4000 cm^{-1} range. The spectra were obtained at a resolution of 4 cm^{-1}.

2.3.2. Liquid range

A differential scanning calorimeter (DSC Q1000 TA-Instruments) with hermetically sealed aluminium pans was used to determine the different state transitions experimented by the pure IL and salt solutions during heating and cooling cycles. All the samples (5——8 mg) were subjected, at least, to four thermal ramps, two in cooling and two in heating mode, with an isothermal step between them:

(a) heating from 25 to 120 °C at 10 °C min^{-1},
(b) isothermal step at 120 °C during 45 min to remove impurities [30] and to erase the thermal history of the sample,
(c) cooling from 120 °C to − 85 °C at 5 °C min^{-1}, followed by an
(d) isothermal step at −85 °C during 5 min, and
(e) heating from −85 °C to 100 °C at 10 °C min^{-1}, and
(f) cooling from 100 °C to −85 °C at 5 °C min^{-1}.

Transition temperatures were determined from the DSC curves, as the onset points of the different peaks, during the reheating and recooling steps following the methodology used in previous papers [31].

A thermogravimetric analyzer (TGA 7-Perkin Elmer) operating in dynamic and isothermal modes under nitrogen and air atmospheres was used to study the thermal stability of the pure IL and the salt solutions. Samples of (3 – 5) mg were placed in an open platinum pan as received, without further purification. Dynamic experiments were performed at temperatures from (100 to 800) °C, with different heating rates, between (1 and 20) °C min^{-1} and with a purge gas flow of 20 cm^3 min^{-1}. Each analysis was repeated three times. The determination procedure of the onset temperatures was reported elsewhere [32]. Furthermore, isothermal TG analysis at temperatures lower than t_{onset} was used to determine the long-term thermal stability of ILs. Both nitrogen and dry air atmospheres were used to analyse their effect on the thermal stability of the selected samples. Curie points of alumel, nickel and perkalloy were used for temperature calibration. With the aim to obtain the purest sample possible of gel by formic acid route, three procedures with small differences in the gel preparation were followed: the first one was the one exposed above, second one performing the gelation under vacuum and later keeping the sample maintain at 80 °C in an oven during 120 min, and the third way was performing the gelation under pressure (3 atm).

2.3.3. Electrical conductivity

Electrical conductivity (σ) has been measured using a conductimeter from CRISON, model GLP31. The resolution of the conductimeter is better than 1 % of the measured value (with a minimum resolution of 2 × 10^{-6} mS cm^{-1}). Before the measurement, bulk IL and mixtures was dried under vacuum for a minimum of 48 h until less than 100 ppm of residual amount of water. All data were measured at least 3 times in different samples to ensure its reproducibility, which was better than 5 % in absolute value. The measuring cells are formed by two parallel plane plates covered with platinum oxide, and were used to measure conductivities in both phases, liquid and gel. The temperature of the samples was controlled using a Julabo F25 thermostat calibrated with an external sensor Crison T-637, which provided a precision better than 0.1 K in the range of measured temperature. It is important to note that all measurements were performed by means of a static isothermal method; in which, the sample was allowed to spend about 15 min at constant temperature before any single measurement was performed, while at the phase transition that period was increased to at least 30 min.

2.3.4. NMR

High resolution magic angle spinning (HRMAS) NMR, which is a technique used to achieve liquid-like (i.e. high resolution) spectra from semi-solid samples, was used to acquire proton spectra of both liquid and gel samples of pure IL and gel and their mixtures with lithium salt 0.1 m. All samples were transferred in a 4 mm ZrO_2 rotor (12.5 μL) for HRMAS and a drop of D_2O was added above the sealing screw for locking. HRMAS NMR spectra were recorded at 11.7 T (corresponding to a ^{1}H operating frequency of 500.13 MHz) using a Bruker DRX 500 spectrometer equipped with a HRMAS probehead and a variable-temperature unit. Spectra were acquired with a spinning rate of 4 kHz to eliminate the dipolar contribution.

To obtain information of the Li nucleus, the mixtures IL + Li 0.1 m and gel + Li 0.1 m were also transferred in standard 5 mm glass tubes for liquid state, high resolution (here indicated as HR NMR to make clear the difference to HRMAS) measurements. HR NMR spectra were recorded in the temperature range 305–330 K at 11.7 T using a Bruker DRX 500 spectrometer equipped with a BBI probehead and a variable-temperature unit. No sample spinning was used. The ^{7}Li operating frequency at the reported magnetic field was 194.3 MHz.

A summary of all samples studied so far is given in Table S1 in the ESI.

^{1}H and ^{7}Li T_1 relaxation times were measured on each sample using data matrices of 32,768 (t_2) x 16 (t_1) complex data points and 4 or 8 transients per increment, with the inversion recovery (IR) pulse sequence. Spectra were acquired in the temperature range 305–330 K and 305–340 K for the liquid and gel samples, respectively. In all experiments, the relaxation delays were set equal or higher than 5 times the longest T_1. The range of variation of the delay time τ was optimised for each experiment and varied in the range 0.005–15 s, 0.01–20 s or 0.01–40 s. The baselines of all arrayed T_1 spectra were corrected prior to

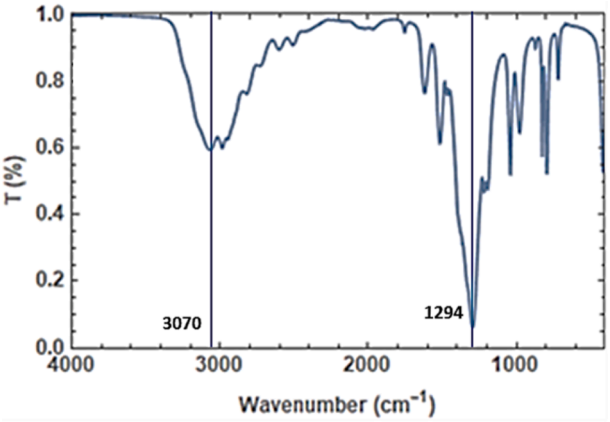

Fig. 1. FTIR spectra of pure EAN.

processing the data using an exponential filter in F_2 dimension (with LB equal to 1.0 Hz). Relaxation times were computed using integrals from experimental raw data by means of the Bruker T_1/T_2 relaxation module using the manual integration option and applying the standard one-component fitting function. Linear fits to extract the rotational activation energies from the relaxation rates were performed with OriginPro 2018.

^{1}H and ^{7}Li self-diffusion coefficients were measured on each sample in the temperature range 305–330 K using data matrices of 32,768 (t_2) x 32 (t_1) complex data points and 8 transients per increment, with the bipolar pulse longitudinal eddy current delay (BPPLED) pulse sequence. A pulsed gradient unit producing magnetic field pulse gradients in the z-direction of 53 G cm^{-1} was used. The pulse gradients were incremented from 2 to 95 % of the maximum gradient strength in a linear ramp. The duration of the magnetic field pulse gradients (δ) and the diffusion times (Δ) were optimized for each sample in order to obtain complete dephasing of the signals with the maximum gradient strength. Overall, δ was varied in the range 1.8–4.0 ms and Δ in the range 0.1–0.45 s.

For ^{1}H experiments, δ values were in the 1.8–4.0 ms range, while Δ values were 0.1–0.45 s long. For ^{7}Li experiments, δ and Δ values were equal to 6.0 ms and 0.8 s, respectively.

Diffusion coefficients were computed from experimental raw data using the Bruker T_1/T_2 relaxation module with the two-component fitting functions.

3. Results

As it is indicated in the introduction section, thermal behaviour of liquid samples doped with lithium salt was already reported by some of us [28], and, although the main objective of this paper is the characterization of the gel state, results of liquid samples will be used for a comparison and a better understanding.

The two gelation routes summarized above were used for the preparation of the pure EAN gels although some bubbles can be observed in the formic acid route. Although some changes in the gelation process were tested to avoid these bubbles, as performing it under low pressure and 80 °C in an oven or with an extra-pressure of 3 atm. at room temperature. Nevertheless, in both cases, the bubbles could not be removed, probably due to the slow evaporation of formic acid. Hence, this work presents thermal analyses and FTIR results of gels obtained by both routes and the electrical conductivity was uniquely determined on the ethanol route gel.

3.1. Infrared spectra

Fig. 1 presents the FTIR spectra of pure EAN, where N–H stretching

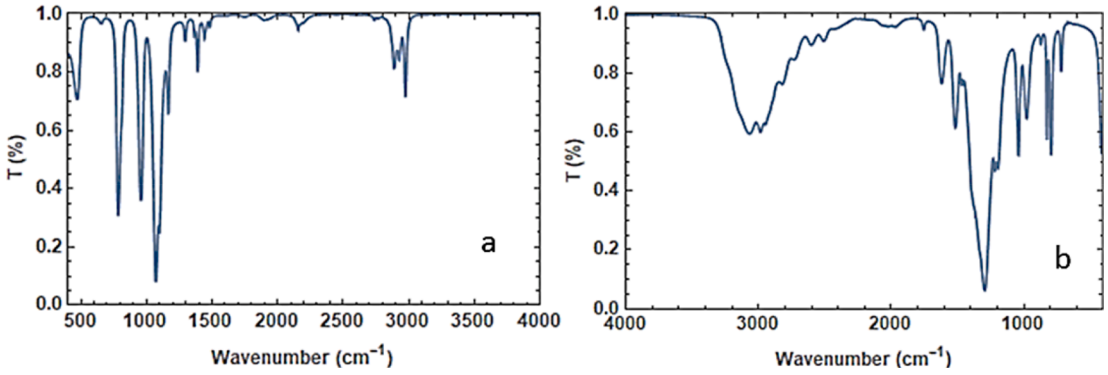

Fig. 2. FTIR Spectra of TEOS (a) and formic acid (b).

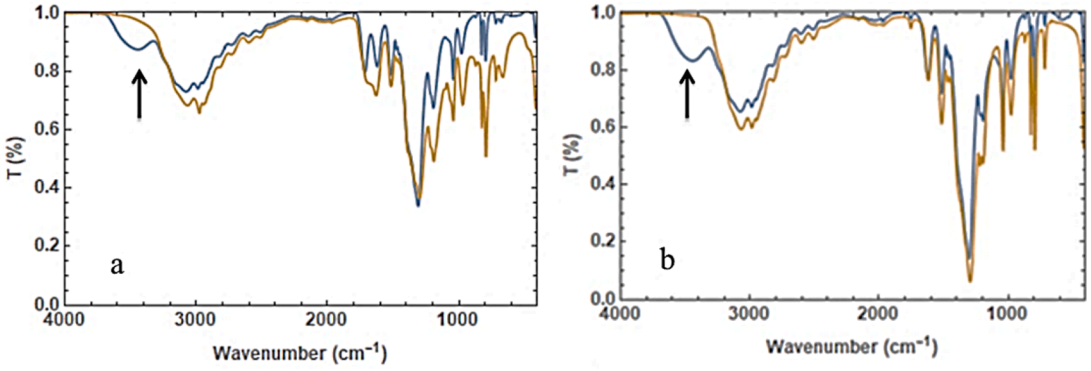

Fig. 3. Comparison between the FTIR spectra of a) ideal mixture approximation (yellow line) and Gel of EAN using the FA route (blue line) and b) ideal mixture approximation (yellow line) and EAN ionogel prepared using the ethanol route (blue line).

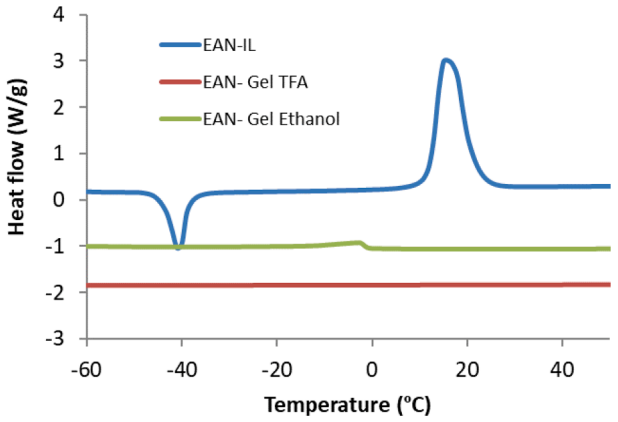

Fig. 4. DSC curves on heating ramp of pure liquid and gel EAN at 5 °C min^{-1}.

leads to the broad band at 3250–2800 cm^{-1} which has contributions of the alkyl CH stretching vibrations producing bands with weaker intensities at 2923 cm^{-1} and 2863 cm^{-1} [33]. The absorption corresponding to N-O bond is observed at 1294 cm^{-1}, while NH_3^+ presents an absorption band at 1619 cm^{-1}. Similarly, spectra of TEOS and formic acid are shown in Fig. 2.

Fig. 3 shows a comparison of the three normalized spectra in Figs. 1 and 2 providing superposition of the compounds of the mixture compared to the ideal mixture without chemical reaction between components (formic acid/ethanol, TEOS and pure EAN). No significant differences in the characteristic peaks of the IL have been observed between the spectra for the different routes. Interestingly, both show a peak at 3600 cm^{-1} attributing to –OH stretching of free water molecules, probably formed during the gelation process [34] or absorbed from the environment due to the highly hydrophilicity of the EAN, as it was widely reported previously [24,35]. This confirms that the characteristic properties of the liquid phase are preserved upon confinement in the silica gel matrix, which, as it will be seen in the following, is confirmed by other experimental techniques employed in this paper.

3.2. Analysis of phase transitions of hydrogel of pure EAN and mixtures

Fig. 4 shows the DSC curve on heating ramp of pure EAN and its silica based gels (two routes). Whereas an exothermic peak at − 44 °C, corresponding to a cold crystallization, followed by a melting peak (endothermic) with onset at 12 °C and peak maximum at 17 °C is observed for pure IL, widely commented in previous paper of our group [28], the gel samples do not present any relevant transitions in the studied

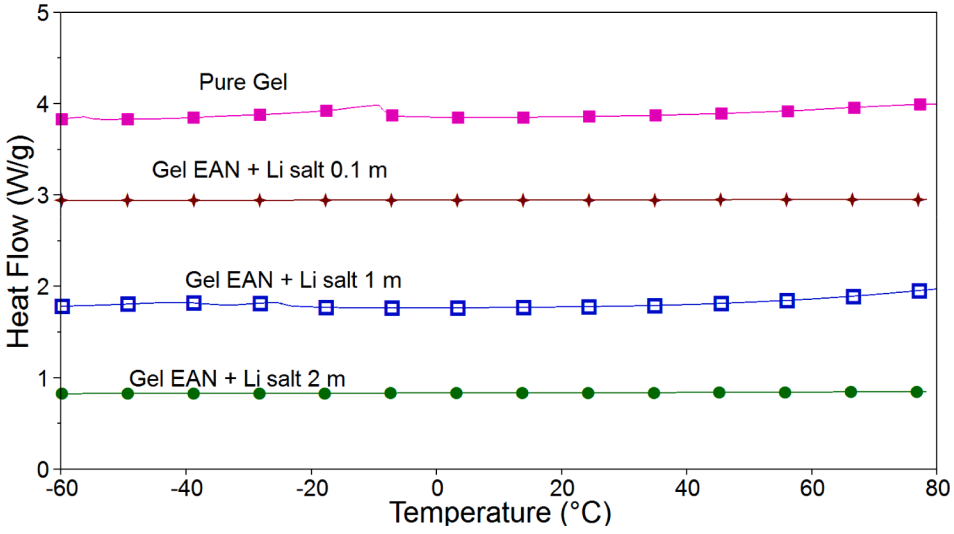

Fig. 5. DSC curves on heating ramp at 10 °C/min of samples EAN + $LiNO_3$ in gel form by ethanol route.

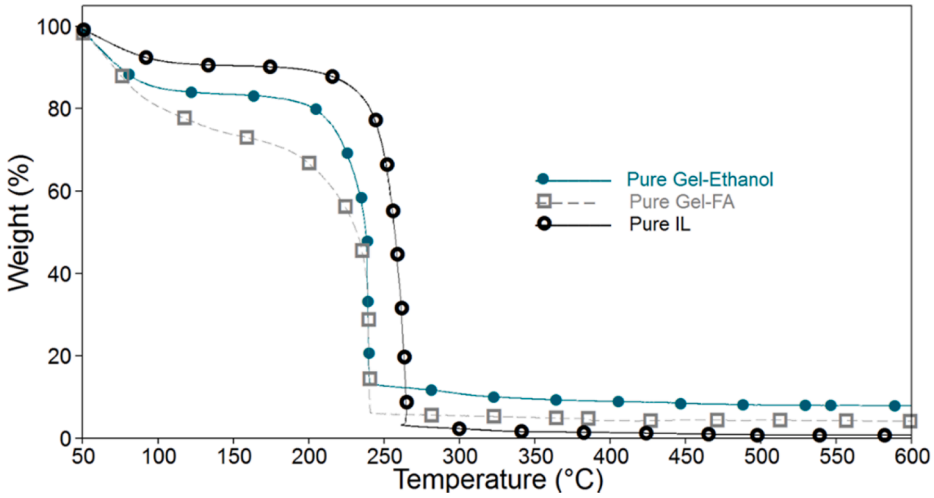

Fig. 6. TG curves of pure liquid and gel EAN.

Table 2
Onset temperature (T_{onset}) and mass loss at 150 °C (Δm(150 °C)) and 450 °C (Δm (450 °C)) for the different samples of pure IL, mixtures IL + $LiNO_3$ in the liquid and gel states. All the experiments were performed in nitrogen atmosphere.

	T_{onset} /°C	Δm(150 °C) /%	Δm(450 °C) /%
Liquid			
EAN without drying	246	9	99
EAN dried	245	3	100
Gel			
EAN without drying (Ethanol)	226	17	92
EAN without drying (FA)	237	8	95
EAN vacuum + heating(FA)	234	3	96
EAN-extra pressure (FA)	235	26	95
EAN + $LiNO_3$ 0.1 m (Ethanol)	231	12	91
EAN + $LiNO_3$ 1.0 m (Ethanol)	230	15	90
EAN + $LiNO_3$ 2.0 m (Ethanol)	230	16	87

ΔU (T_{onset}) = 6 °C, **ΔU** (Δm) = 1 %.

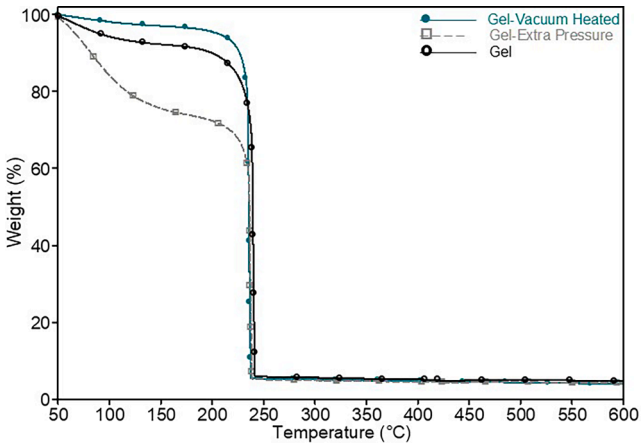

Fig. 7. TG curves of gels of EAN corresponding to the three different procedures of formic acid route.

temperature interval.

Likewise, no thermal transitions are observed neither upon heating nor upon cooling of confined saturated solutions of metal salts in EAN in the explored temperature range, as can be seen in Fig. 5, which shows the DSC profiles on heating ramp at 10 °C·min^{-1} of these samples. The same behaviour is observed in the cooling ramps for the studied mixtures.

These DSC results showed that the phase behaviour of the IL is notably altered upon confinement. Specifically, the crystallization upon cooling, the cold crystallization and the subsequent melting upon heating are suppressed for all the confined samples in the studied temperature interval. This response was also observed by Garaga *et al.* [19], who studied the ionic mobility of gels based on robust nanoporous silica micro-particles and two ILs namely one aprotic imidazolium, 1-methyl-3-hexylimidazolium bis(trifluoromethanesulfonyl)imide, and one protic ammonium, diethylmethylammonium methanesulfonate. The constraints due to confinement prevent solid-state organization of the IL and liquid mixtures at low temperature [21]. The same behaviour is observed upon salt addition [28], which also frustrates crystallization by avoiding the formation of IL cation–anion complexes. This is probably due to the strongly electrostrictive metal cations in the polar regions, which give rise to the formation of $[Li(NO_3)_4]^{3-}$ complexes in the polar regions [18].

3.3. Thermal stability analysis

Fig. 6 shows the comparison between the thermogravimetric curves (TG) of pure EAN in liquid and gel states without previous purification. An important mass loss until 150 °C took place due to evaporation of free water and volatile precursors of the gelation. TG curves are characterized by a step starting at 175 °C and finishing at 275 °C with a single peak in the corresponding DTG curve. The onset temperature of gelled samples is slightly lower than that of the pure IL, suggesting that the confinement in the silica scaffold does not affect significantly the thermal stability of the IL. Table 2 summarizes the onset temperature, mass loss at 150 °C and 450 °C of all these samples. Additionally, no dependence of the IL thermal stability with the atmosphere (N_2 and air) has been observed, suggesting that a common oxygen-independent mechanism (evaporation) is behind this process [28].

Fig. 7 shows the TG curves of EAN gel after these three different procedures; the results indicated that the onset temperature is not dependent on the way the gel is prepared and it is the same as that of the pure IL. Our results are in good agreement with those of previous researchers [19,29,36]. The only difference is that the first step disappeared with the gelation under vacuum and a subsequent heating at 80 °C, as it can be expected because the most volatile substances are evaporated before the TG experiments. These gelled samples were later used for measurements of the electrical conductivity to avoid any relevant influence of spurious volatiles.

Regarding the effect of the Li salt, Fig. 8 shows the corresponding TG curves and the onset temperature and the mass loss at 150 °C and 450 °C were also indicated in Table 2. The salt addition has no appreciable effect on the onset temperature, as it happened in the liquid mixtures

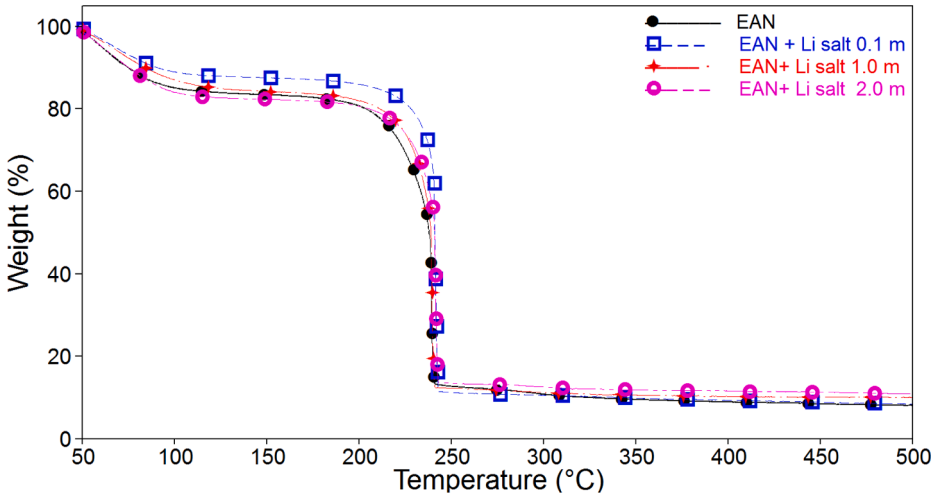

Fig. 8. TG curves of EAN gel doped with different concentrations of Li salt, prepared by the ethanol route.

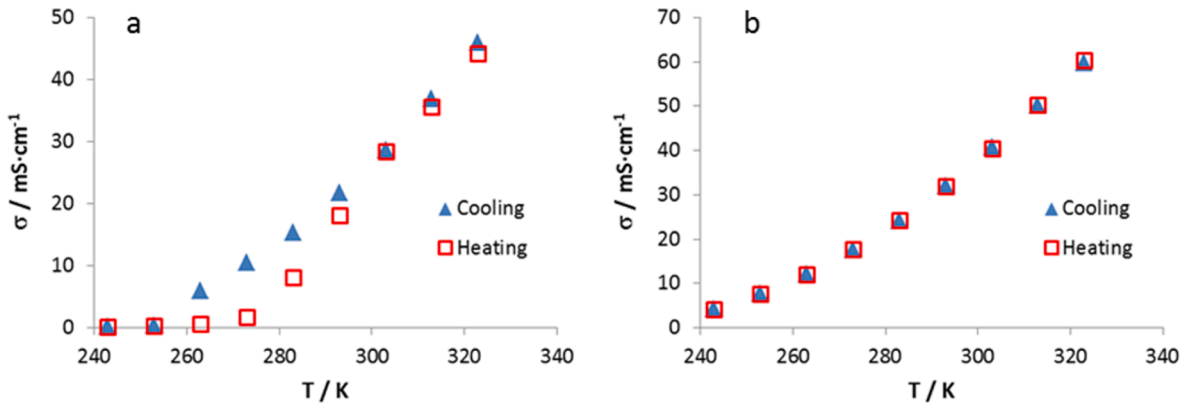

Fig. 9. Electrical conductivity against temperature of pure EAN in the liquid (a) and in gel (by ethanol) (b) states.

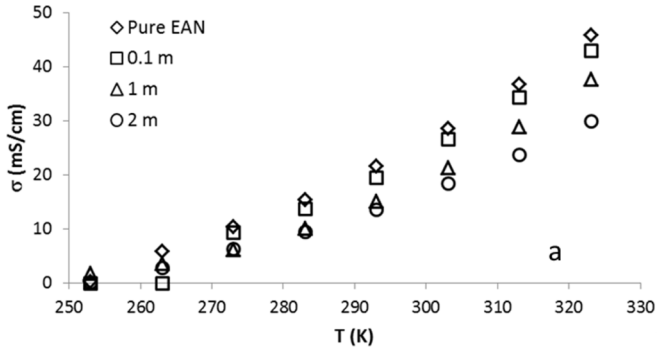

Fig. 10. (a) Electrical conductivity versus temperature of liquid mixtures EAN + Li NO_3.

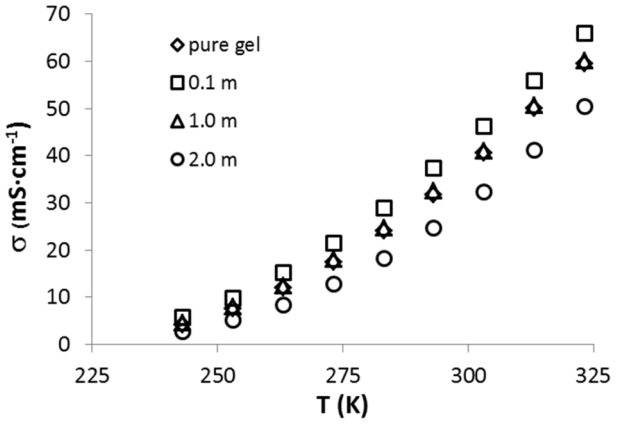

Fig. 11. Electrical conductivity of gel mixtures of EAN and lithium nitrate at the four studied concentrations.

reported in a previous work [28]. Only a reduction in mass loss (in %) at 150 °C, due to the evaporation of water and ethanol is observed. An increase of mass loss at 450 °C due to salt residue at this temperature is visible, being also observed in liquid mixtures [28].

3.4. Ionic conductivity

The effect of the addition of the lithium salt and that of the gelation on ionic conductivity study were analysed, and the results are summarized in this section. Results are presented in Table S2 (ESI). This property was studied as a function of the temperature and lithium salt concentration in both bulk liquid state and confined in a silica scaffold.

Firstly, Fig. 9 shows a comparison between the electrical conductivity of pure EAN in liquid (a) and gel (ethanol) states (b) in the temperature interval (243.15 – 323.15) K, upon cooling down and heating up scanning. Up to our knowledge no values of EAN silica ionogels have been previously reported and values of pure liquid EAN are in good agreement with the literature [16,37,38]. Besides the highest values of conductivity in the gel state, a clearly visible hysteresis loop in liquid state, absent in the gel state in the studied temperature interval, is the most remarkable observation. This hysteresis is coherent, and even expected, with the supercooling effect observed in the DSC results of pure liquid EAN with a melting peak at 285 K determined within heating scans and a freezing peak at 246 K upon the cooling ramps [28]. In addition, the thermal behaviour of gel samples, without first order transitions in the entire temperature interval analysed, explains the results of this property obtained for the gelled samples. Current lithium salt solutions used in lithium-ion batteries show conductivity values ca. 10 mS/cm, similar to our results [39].

On the other hand, Fig. 10 shows the electrical conductivity of liquid mixtures at different concentrations of lithium salt in the IL. Besides the disappearance of the hysteresis loop found in the pure IL, salt addition decreases conductivity and, increases the viscosity, as it has been probed in recent literature [16,24,40]. This agrees well with the behaviour of classical electrolyte solutions and mixtures of others ILs with different metal salts, where the conductivity is proportional to the density of charge carriers and inversely proportional to viscosity, as it is widely reported in the literature [39,41–44].

On the other hand, Fig. 11 shows the ionic conductivity of gels of EAN and of its mixtures with lithium nitrate at the four studied concentrations. As can be expected, and similarly to liquid samples, this parameter increases with temperature. Nevertheless, in what regards the dependence of conductivities in salt concentration, important differences are observed: the highest values of conductivity correspond to the gel doped with the lowest salt concentration, intermediate concentrations of lithium salt present similar values to those of the pure EAN gel and the saturated gel shows the lowest values of conductivity. This fact could be explained as follows: at low concentration the salt is fully available for conductivity but increase in the salt concentration leads to complexation that makes the salt unavailable to conduction. This hypothesis will be evaluated in the next section of the paper.

It is especially interesting that for all the salt concentration, the highest values of the ionic conductivity correspond to the gel samples for all the temperatures as can be seen in Figure S1 of supplementary material, which shows the Arrhenius plot for all the samples. This behaviour is not unanimously reported in the literature, and some controversial results have been communicated. Noor *et al.* [29] established that the ionic conductivity of ionogels of 1-butyl-3-methyl imidazolium tetrafluoroborate with different amount of TEOS decreases as the amount of silica increases, being the hydrogen bond networks

Table 3
Fitting parameters of the VFT equation for pure EAN and its mixtures with lithium salt in liquid and gel states. Error values are determined by fitting procedure.

	$A = \ln(\sigma_0)$	B / K	T_0 / K
Liquid form			
Pure IL	7.1 ± 0.3	530 ± 70	163 ± 9
0.1 *m*	7.4 ± 0.2	610 ± 50	155 ± 6
1.0 *m*	7.7 ± 0.2	650 ± 30	161 ± 3
2.0 *m*	6.8 ± 0.1	530 ± 30	164 ± 4
Gel form			
Pure IL	6.94 ± 0.04	474 ± 10	157 ± 2
0.1 *m*	6.70 ± 0.04	409 ± 9	160 ± 2
1.0 *m*	7.11 ± 0.05	523 ± 13	149 ± 2
2.0 *m*	7.22 ± 0.06	567 ± 17	151 ± 2

between BF_4^- and the hydroxyl group in the silica the mechanism of IL immobilization suggested by these authors. On the contrary, Le Negre *et al.* [23] and Sajid *et al.* [45] found similar or even higher values of the ionic conductivity of ionogels of N, N, N triethyl octyl ammonium bromide relative to neat IL in the temperature interval between 253 K and 333 K, which evidences the relatively small impact of the silica scaffold in this property, as it happens here, for the gel of lowest salt concentration. In addition, and taking into account the importance of impurities in ionic conductivity, an appropriate assessing the presence of traces of gel precursors or molecular compounds generated during the sol–gel synthesis, and the possible water absorption during preparation, is fundamental, as well as knowing how these traces affect the results. This is exposed in the next section of this work.

The temperature dependence of conductivity is usually described by the Arrhenius law. Nevertheless, in many cases, particularly for ILs, a non-linear behaviour of ln σ against (1/T) shows that an Arrhenius behaviour is not followed in the studied temperature range, and a Vogel–Tammann–Fulcher equation (eq. (1) must be applied [45–48].

$$ln\sigma = A - \frac{B}{T - T_0} \quad (1)$$

where A is the conductivity at infinite temperature, and it assumed to be proportional to the number of charge carriers. B is the fragility index or strength index, which is inversely proportional to the kinetic fragility of the liquid, and T_0 is the vanishing mobility temperature, also known as the Vogel temperature (or ideal glass transition temperature). As it is well-known, these dense ionic systems exhibit, in general, a thermal activation of the VFT type [48], which is associated to the presence of several relaxation times in the underlying dynamics, characteristic of disordered systems. On the other hand, the Vogel temperature can be related with the glass transition temperature (T_g), verifying $T_0 < T_g$ [39], for slow processes, which is approximately the case in this work. Fitting parameters of our results to the VFT equation (eq. (1)) are presented in Table 3 for the liquid and gel samples. This behaviour is usually observed in bulk ILs, but it was also found by other authors in gel states, suggesting a common vehicular mechanism of charge transport [19].

As it can be seen, for the liquid samples the conductivity at infinite temperature remains nearly constant with the concentration of lithium salt until 1.0 m, and presents the lowest value for the highest salt concentration. Despite the similar values obtained in fitted parameters (T_0 and B), T_0 (the ideal glass transition temperature) tends to increase while increasing salt concentration in liquid samples. This could be explained by an increase of the fragility index with increasing salt concentration in the studied mixture due a "softening" in the internal structure of the sample.

On the other hand, the conductivity at infinite temperature and the fragility index tend to decrease with the gelation for pure IL and mixtures of 0.1 and 1 m, whereas both parameters increase after gelation for the sample with the highest concentration of salt. The T_0 values tend to decrease because of gelation, as thermal analysis study also indicates. In this case, the fragility index is increasing with the salt concentration for gel samples, which is traduced in a decrease of the ideal glass transition temperature (T_0).

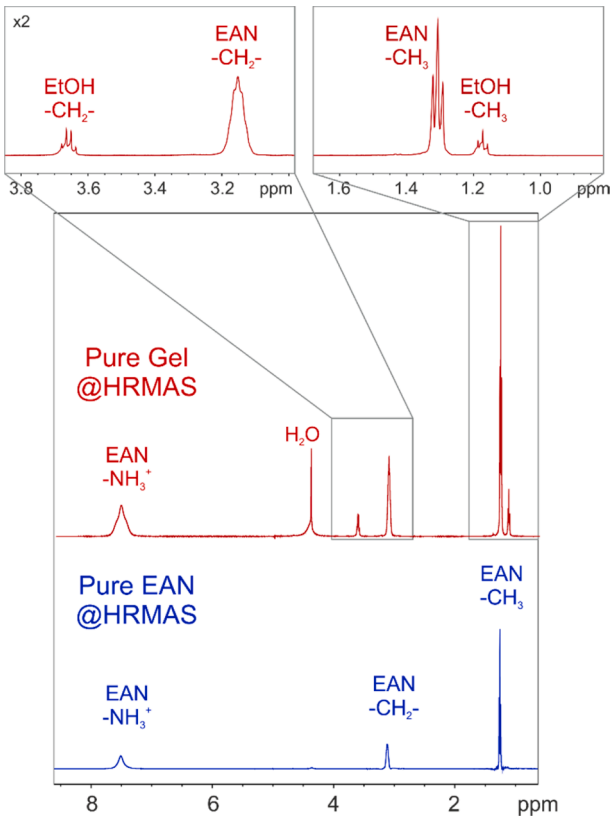

Fig. 12. 1D ^{1}H HRMAS NMR spectra of pure EAN (bottom, blue) and pure gel of EAN (top, red) measured at 305 K. Enlargement of the regions corresponding to the methylene and methyl protons are also shown for the pure gel.

As it is well known, fragility index is related to molecular mobility, and latter to ionic conductivity [49]. This fact can be seen on B parameter summarized in Table 3. Gel samples present lower fragility index, which may be due to confinement confering higher resistance to structural rearrangements over temperature than that in liquids samples [47]. Guyomard-Lack *et al.* [49] also reported lower values on fragility index when the IL + Li salt is confined, and noticed that fragility is highly dependent on the pore size. This behaviour could be explained by the formation of nanosolids in the polar cavities of the IL at the highest salt concentration, as it was pointed out in previous works of our research group [18,24]. Results show that the confinement of the liquid mixtures allows maintaining the liquid properties and it seems that lithium salt addition changes the solvation, provoking that Li^+ electrostriction capture NO_3^- anions freeing IL cation. For a better understanding of it, high resolution magic angle spinning NMR studies of these samples were performed and they are exposed in the next section of this work.

3.5. NMR studies

With the aim to clarify the effect of gelation and salt addition, NMR studies using high resolution magic angle spinning (HRMAS) technique were performed in liquid and gel samples (by ethanol route) of pure EAN and mixture of EAN + $LiNO_3$ at 0.1 m concentration. This not so common and special NMR technique makes it possible to achieve liquid-like (i.e. high resolution) spectra from gelled samples [50]. The dramatic increase in resolution that can be obtained with HRMAS NMR applied to gel of EAN can be appreciated in Fig. S2.

Fig. 12 shows the ^{1}H HRMAS NMR spectra at 305 K of gel of pure

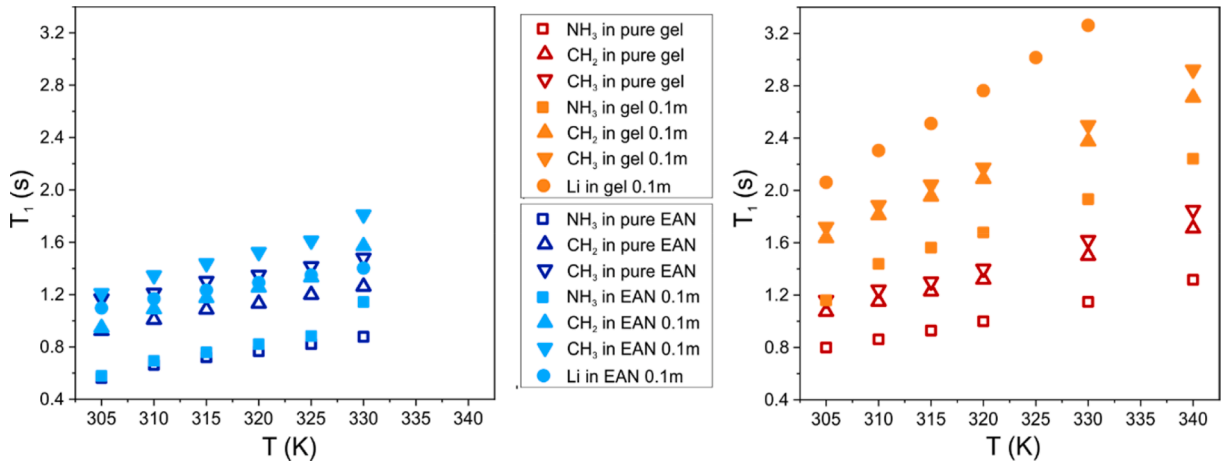

Fig. 13. ^{1}H and ^{7}Li T_1 relaxation times measured as a function of temperature for each sites (NH_3, square; CH_2, triangle; CH_3, inverted triangle; Li, circle) of liquid (left) and gel (right) samples, with (filled symbols) and without (empty symbols) Li salt.

EAN (by the ethanol route) and pure liquid EAN, which immediately reveal that in the gel sample, next to the three signals corresponding to the EA^+ cation, there are also the signals of the methylene and methyl protons of the residual ethanol as well as a residual water peak. It can be estimated that the EtOH and water content in the ionogel are of ca. 3 wt % and 4 wt%, respectively.

These non-negligible amounts of water and ethanol, residues of the sol–gel process, can be the cause of the high values of conductivity in gel samples, especially the water content as different authors have been previously reported, with increases of 50 % in this property with the addition of less than 4 % of water in liquid samples of butylmethylpyrrolidinum bistrifluromethylsulfonylimide (BMPyrr TFSI) [51] and EAN [52]. To try to discern the effect of confinement from the effect of these impurities in gel samples, the conductivity of the liquid samples, pure IL and mixtures with Li salt, with 4 % water, and with both 4 % of water and 3 % of ethanol was determined at 20 °C. Results are enclosed in Fig. S3 of ESI, showing that the conductivity increases substantially (more than 50 %) with the water addition in all the cases, as can be expected, and the highest rise corresponds to the sample doped with the highest concentration of lithium nitrate, with a change from 13.4 to 23.9 mS/cm after the addition of water. Also the ethanol provokes a slight increase in all the liquid samples. Nevertheless, the most important and interesting result is that the values of the ionic conductivities in gel samples are similar (or slightly lower) than the values of liquid samples of EAN with water and ethanol and, even, slightly higher than the corresponding values of the liquid mixtures of IL + Li salt with water and ethanol. These findings corroborate the idea that ionogels preserve the liquid behaviour after the confinement.

To get insights into the local mobility of the species, proton spin–lattice relaxation times, T_1, were measured for the gel and liquid samples by HRMAS NMR (Table S3 and Fig. 13). To analyse the effect of lithium salt, T_1 values for ^{7}Li were also measured for the liquid and gel EAN mixtures with 0.1 m $LiNO_3$ salt by conventional solution state NMR (Table S4 and Fig. 13). As expected, T_1 values increase with increasing temperature for all curves.

The effect of gelation on the overall dynamics of the components can be summarized as follows:

- The gelation increases the T_1 values for all proton and lithium sites in both samples (with and without the addition of $LiNO_3$), but the effect is much greater in the mixture with the lithium salt (Fig. 13, orange vs light blue).
- In the liquid mixture with the lithium salt, lithium shows T_1 relaxation times which are similar to the alkyl protons of EAN, while in the ionogel, the T_1 values for lithium are the highest measured values.

Table 4
^{1}H and ^{7}Li activation energy for the rotational motion.

Species	E_a^{rot}(kJ mol^{-1})	Species	E_a^{rot}(kJ mol^{-1})
NH_3^+ in pure EAN	11.7	NH_3^+ in pure gel	12.3
CH_2 in pure EAN	9.3	CH_2 in pure gel	11.5
CH_3 in pure EAN	8.0	CH_3 in pure gel	11.5
NH_3^+ in EAN 0.1 *m*	13.5	NH_3^+ in gel 0.1 *m*	12.8
CH_2 in EAN 0.1 *m*	11.3	CH_2 in gel 0.1 *m*	12.1
CH_3 in EAN 0.1 *m*	10.0	CH_3 in gel 0.1 *m*	12.7
Li^+ in EAN 0.1 *m*	8.2	Li^+ in gel 0.1 *m*	15.3

Even if a direct comparison between the relaxation times of protons and lithium is not possible due to the different dominating relaxation mechanism (dipolar versus quadrupolar), these observations point towards a major effect of the gelation on the local rotational motion of all species in the mixture. Notably, this strong effect passes through a direct involvement of the lithium cation whose rotational motion is strongly correlated to the EAN cation in the liquid system, while it diverges significantly in the ionogel. The dynamics of Li^+ is then strongly linked to gelation, and this emerges indeed also considering more closely the effect of the addition of the lithium salt to the neat EAN and the ionogel: The presence of $LiNO_3$ does not have any relevant effect on the liquid system (see Fig. 13, left panel where empty and filled symbols are clustered) but significantly increases the T_1 values of all EAN protons in the ionogel (see the broad distribution of the filled symbols in Fig. 13, right panel) Overall, the combined effect of lithium salt and gelation results in the selective and broad enhancement of the relaxation process of lithium ions (orange filled circles in Fig. 13, right).

Considering the linear behaviour of the T_1 trends in the given temperature interval, the rotational activation energy was calculated using the Arrhenius approximation (extreme narrowing condition) [53,54]:

$$T_1 = T_{1,A} exp\left(\frac{E_a^{rot}}{RT}\right) \quad (2)$$

where $T_{1,A}$ is a pre-exponential factor, R the gas constant, T the absolute temperature and E_a^{rot} the apparent activation energy for the rotational motion. E_a^{rot} are reported in Table 4, and Arrhenius plots are displayed in Fig. S4.

In both the pure EAN and its mixture with $LiNO_3$, the rotational activation energy for the EAN protons follows the order $NH_3^+ > CH_2 > CH_3$. After gelation all E_a^{rot} basically level out: the incorporation into the

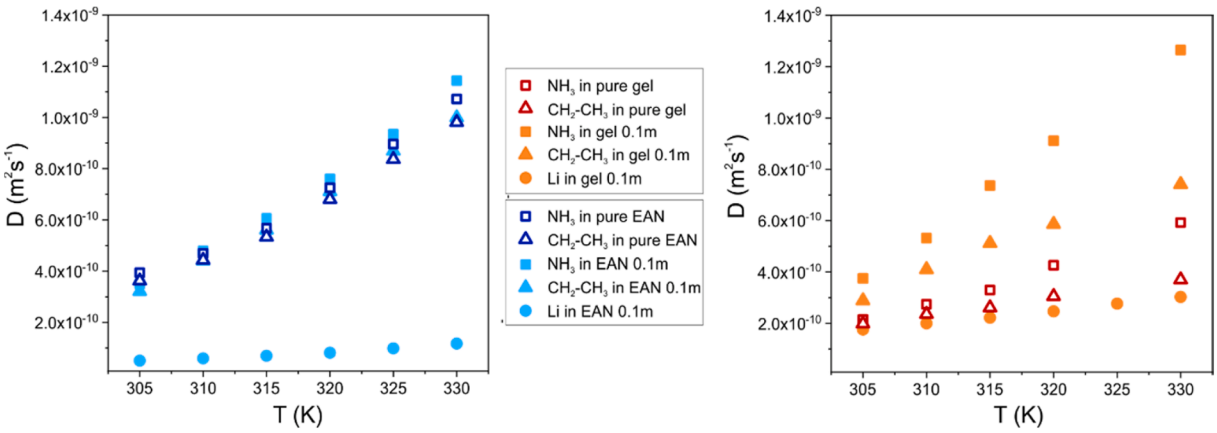

Fig. 14. ^{1}H and ^{7}Li apparent self-diffusion coefficients measured as a function of temperature for the different species (NH_3, square; CH_2-CH_3 triangle; Li, circle) in liquid (left) and gel (right) samples, with (filled symbols) and without (empty symbols) Li salt. For the gel samples, only the more reliable and abundant component is reported.

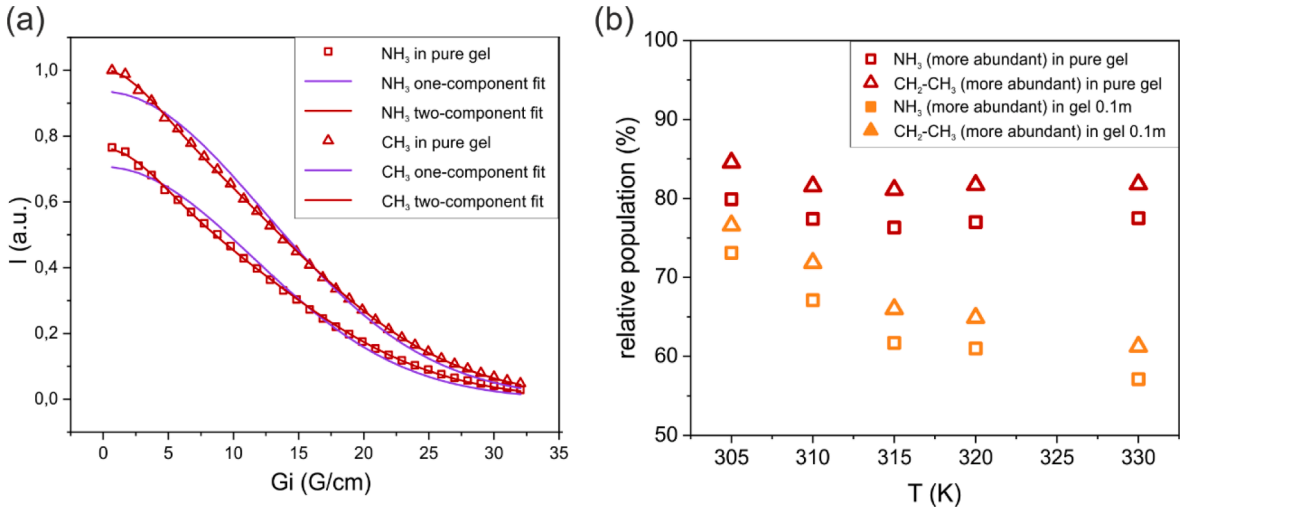

Fig. 15. (a) Diffusion decays measured by PFG-NMR for protons NH_3^+ and CH_3 acquired in the pure gel of EAN at 305 K and corresponding fits using a mono- or a bi-exponential function, plotted as a function of the gradient strength; (b) Relative percentage of the more abundant components of the NH_3^+ and alkyl (CH_2 and CH_3) protons of EAN, obtained for the pure gel and the mixture with $LiNO_3$ 0.1 m via a bi-exponential fit of the diffusion decays.

gel structure makes the barrier for the rotational motion almost equal for all protons.

As for the effect of the addition of lithium salt, it causes an overall increase of the rotational activation energy for all protons.

Apparent self-diffusion coefficients were obtained for both protons and lithium by pulsed field gradient (PFG)-NMR experiments (Fig. S5 and S6 and Fig. 14 and Fig. S5).

Studying the diffusion behavior in such complex gel systems is challenging, as genuine molecular diffusion, exchange and confinement all contribute to the measured diffusion coefficient. Some important observations help in dissecting the different processes.

The diffusion coefficient of the NH_3^+ protons is slightly higher than that corresponding to the CH_2 and CH_3 protons in all samples, both liquid and gel system, with and without lithium salt. As diffusion is a molecular property, the difference in diffusion between the ammonium head and the alkyl chain of the cation EA^+ indicates that exchange plays always a role, and this occurs not only among NH_3^+ protons (which are the only exchangeable protons in the liquid system) but probably also includes EtOH and H_2O labile protons (which are also present in the gel samples).

Unlike liquid samples, where a mono-exponential decay was observed for all EAN protons (both with and without $LiNO_3$), in the two gel samples (with and without $LiNO_3$) the observed proton diffusion decays for both EAN cation and EtOH are not mono-component decays. The analysis of the multiexponential diffusion decays was then performed via the Bruker T_1/T_2 module using a two-component fitting function. In all cases, a bi-exponential model could reproduce the decays, as reported for instance in Fig. 15a for the ammonium and methyl protons of the cation in the pure gel at 305 K. Unlike protons, lithium is mono-exponential in both the liquid and gel mixture.

Broadly speaking, the biexponential fit observed for the cation EA^+ is compatible with heterogeneity within the gel matrix [55,56]. Only the apparent diffusion coefficients and the relative percentage obtained for the more abundant component are reported in Table S5 and Fig. 14. Given the large error associated to the less abundant component, the latter has been interpreted here not as a physically meaningful fraction of molecules, but as a symptom of a heterogeneous soft matrix. If one looks at the relative population (Fig. 15b), it can be observed that the relative amount of the more abundant component is more or less stable over the T interval for the pure gel sample, while it is reduced of about 15 % from 305 K to 330 K for both NH_3^+ and alkyl protons of Gel 0.1 m.

Bearing in mind the effects of exchange and confinement, further considerations can be drawn looking again at data of Fig. 14, trying to separately evaluate the effect of gelation and Li-doping:

- The gelation decreases the diffusion coefficient of both NH_3^+ and alkyl protons in the samples without lithium (blue vs red empty symbols). This is intuitively explained considering the formation of a more viscous interacting system. The same effect is observed for the CH_2 and CH_3 protons of EAN when the IL plus lithium salt mixture is gellified (light blue vs orange filled triangles).
- Interestingly, the diffusion of NH_3^+ protons of the EAN + $LiNO_3$ shows an increase in self-diffusion coefficient after formation of the gel (light blue vs orange filled squares). This may be related to a rise in the exchange process due to the presence of residual EtOH and H_2O or some other additional process.
- Lithium is the slowest diffusing species both in liquid and gel mixture (light blue vs orange filled circles). Its self-diffusivity increases after gelation, but it is anyway much lower than NH_3^+ and alkyl protons of EAN.
- The effect of Li-doping is almost null in the liquid system (left) but significant in the gel, as the apparent diffusivity of both proton species of the cation increases (right). In other words, the more abundant component of the NH_3^+ and alkyl protons in the ionogel diffuses much faster in the presence of $LiNO_3$. This confirms the observation of the thermal analysis, which lead to the conclusion that the presence of metal cations in low concentration frustrates the crystallization of EAN in the heterogeneous gel matrix, freezing the IL cations and lithium-anions complexes are formed.

4. Conclusions

This work analyses the effect of the confinement on a silica scaffold of the protic IL, EAN and its mixtures with lithium nitrate in terms of thermal behaviour, ionic conductivity and ion mobility from high resolution magic angle spinning NMR analysis.

Our main conclusions are:

- Both, confinement and salt addition frustrate the crystallization of all the mixtures, inducing an amorphous behaviour in all the samples. No significant changes on the thermal stability of the mixtures were detected regarding the bulk EAN.
- Ionic conductivity of liquid samples shows the expected behaviour, but this magnitude increases up to a maximum in the doped sample with the lowest concentration $LiNO_3$ in gel samples, although this rise can moderately be attributed to the traces of sol–gel precursors. Nevertheless, the most important finding in this work is that the confinement does not reduce the ionic conductivity of the liquid encapsulated in the silica scaffold, and the liquid behaviour is maintained in the ionogel.
- High resolution magic angle spinning NMR shows that the addition of lithium nitrate increases the mobility (both rotational and translational motion) of the cation EA^+ within the ionogel. The bi-exponential decay observed for the apparent diffusion of the cation gives evidence of the presence of two different populations, fact that can be interpreted as a signal of heterogeneity in the soft matrix, marking a substantial difference with the pure ionic liquid, where a mono-exponential behaviour is observed. The Li^+ cation also displays a higher mobility (both rotational and translational motion) in the ionogel than in the neat ionic liquid.
- Results show that the confinement of the liquid mixtures allows maintaining the liquid properties and the lithium salt addition changes the solvation, provoking that Li^+ electrostriction capture NO_3^- anions freeing IL cation.
- Our observations indicate that Li^+ does not interact with the polymer matrix in these silica-based gels.

Declaration of competing interest

The authors declare that they have no known competing financial interests or personal relationships that could have appeared to influence the work reported in this paper.

Data availability

Data will be made available on request.

Acknowledgements

Authors acknowledge M. Gómez (RIAIDT-USC) for the technical support in DSC measurements. This work was supported by Spanish Ministry of Economy and Competitiveness and FEDER Program through the projects MAT2017-89239-C2-1-P and MAT2017-89239-C2-2-P and the SISE Network RED2018-102679-T as well as by Xunta de Galicia through GRC ED431C 2020/10 project and the Galician Network of Ionic Liquids (ReGaLIs) ED431D 2017/06. P. Vallet and J. J. Parajó thank funding support of FPI Program from Spanish Ministry of Science, Education and Universities and I2C postdoctoral Program of Xunta de Galicia, respectively.

Appendix A. Supplementary data

Supplementary data to this article can be found online at https://doi.org/10.1016/j.molliq.2024.124093.

References

[1] T. Vogl, S. Menne, A. Balducci, Mixtures of protic ionic liquids and propylene carbonate as advanced electrolytes for lithium-ion batteries, PCCP 16 (2014) 25014–25023, https://doi.org/10.1039/c4cp03830d.
[2] O. Russina, R. Caminiti, T. Méndez-Morales, J. Carrete, O. Cabeza, L.J. Gallego, L. M. Varela, A. Triolo, How does lithium nitrate dissolve in a protic ionic liquid? J Mol Liq 205 (2015) 16–21, https://doi.org/10.1016/j.molliq.2014.08.007.
[3] H. Porthault, C. Calberg, J. Amiran, S. Martin, C. Páez, N. Job, B. Heinrichs, D. Liquet, R. Salot, Development of a thin flexible Li battery design with a new gel polymer electrolyte operating at room temperature, J Power Sources 482 (2021), https://doi.org/10.1016/j.jpowsour.2020.229055.
[4] J.J. Parajó, P. Vallet, L.M. Varela, M. Villanueva, J. Salgado, Ecotoxicity of binary mixtures of ILs and inorganic salts of electrochemical interest, Environ. Sci. Pollut. Res. (2021), https://doi.org/10.1007/s11356-021-17515-1.
[5] J.J. Parajó, J.M. Otero-Mato, A.I.M.C. Lobo Ferreira, L.M. Varela, L.M.N.B. F. Santos, Enthalpy of solvation of alkali metal salts in a protic ionic liquid: Effect of cation charge and size, J Mol Liq 360 (2022), https://doi.org/10.1016/j.molliq.2022.119228.
[6] T. Stettner, P. Huang, M. Goktas, P. Adelhelm, A. Balducci, Mixtures of glyme and aprotic-protic ionic liquids as electrolytes for energy storage devices, J. Chem. Phys. 148 (2018) 193825–193831, https://doi.org/10.1063/1.5013117.
[7] D.R. MacFarlane, N. Tachikawa, M. Forsyth, J.M. Pringle, P.C. Howlett, G. D. Elliott, J.H. Davis, M. Watanabe, P. Simon, C.A. Angell, Energy applications of ionic liquids, Energy Environ. Sci. 7 (2014) 232–250, https://doi.org/10.1039/C3EE42099J.
[8] M.E. Van Valkenburg, R.L. Vaughn, M. Williams, J.S. Wilkes, Thermochemistry of ionic liquid heat-transfer fluids, Thermochim Acta 425 (2005) 181–188, https://doi.org/10.1016/j.tca.2004.11.013.
[9] H. Qin, M.J. Panzer, Chemically cross-linked poly(2-hydroxyethyl methacrylate)-supported deep eutectic solvent gel electrolytes for Eco-friendly supercapacitors, ChemElectroChem 4 (2017) 2556–2562, https://doi.org/10.1002/celc.201700586.
[10] J. Brad Shotwell, R.A. Flowers, Electrochemical investigation of the solvolytic properties of ethylammonium nitrate (EAN) and propylammonium nitrate (PAN), Electroanalysis 12 (2000) 223–226, https://doi.org/10.1002/(sici)1521-4109(200002)12:3<223::aid-elan223>3.0.co;2-y.
[11] J.A. Garlitz, C.A. Summers, R.A. Flowers, G.E.O. Borgstahl, Ethylammonium nitrate: A protein crystallization reagent, Acta Crystallogr D Biol Crystallogr 55 (1999) 2037–2038, https://doi.org/10.1107/S0907444999011774.
[12] D. Yalcin, A.J. Christofferson, C.J. Drummond, T.L. Greaves, Solvation properties of protic ionic liquid-molecular solvent mixtures, PCCP 22 (2020) 10995–11011, https://doi.org/10.1039/d0cp00201a.
[13] R. Zarrougui, M. Dhahbi, D. Lemordant, Volumetric properties of ethylammonium nitrate + γ-butyrolactone binary systems: Solvation phenomena from density and raman spectroscopy, J Solution Chem 39 (2010) 1531–1548, https://doi.org/10.1007/s10953-010-9600-3.
[14] M.E. Gliege, W.J. Lin, Y. Xu, M.T. Chen, C. Whitney, R. Gunckel, L. Dai, Molecular dynamics insight into the role of water molecules in ionic liquid mixtures of 1-Butyl-3-methylimidazolium iodide and ethylammonium nitrate, J. Phys. Chem. B 126 (2022) 1115–1124, https://doi.org/10.1021/acs.jpcb.1c05595.
[15] M. Otero-Lema, P. Martínez-Crespo, T. Méndez-Morales, H. Montes-Campos, L. M. Varela, Interfacial structure of protic and aprotic ionic liquid-DMSO-Li salt

mixtures near charged and neutral electrodes: A Molecular Dynamics study, J Mol Liq 386 (2023), https://doi.org/10.1016/j.molliq.2023.122492.
[16] A. Filippov, A.S. Alexandrov, R. Gimatdinov, F. Ullah Shah, Unusual ion transport behaviour of ethylammonium nitrate mixed with lithium nitrate, J Mol Liq 340 (2021), https://doi.org/10.1016/j.molliq.2021.116841.
[17] V.V. Matveev, A.V. Ievlev, M.A. Vovk, O. Cabeza, J. Salgado-Carballo, J.J. Parajó, J.R. Rodríguez, R. de la Fuente, E. Lähderanta, L.M. Varela, NMR investigation of the structure and single-particle dynamics of inorganic salt solutions in a protic ionic liquid, J Mol Liq 278 (2019) 239–246, https://doi.org/10.1016/j.molliq.2019.01.010.
[18] T. Méndez-Morales, J. Carrete, Ó. Cabeza, O. Russina, A. Triolo, L.J. Gallego, L. M. Varela, Solvation of lithium salts in protic ionic liquids: A molecular dynamics study, J. Phys. Chem. B 118 (2014) 761–770, https://doi.org/10.1021/jp410090f.
[19] M.N. Garaga, L. Aguilera, N. Yaghini, A. Matic, M. Persson, A. Martinelli, Achieving enhanced ionic mobility in nanoporous silica by controlled surface interactions, PCCP 19 (2017) 5727–5736, https://doi.org/10.1039/c6cp07351d.
[20] C. Xu, Q. Dai, L. Gaines, M. Hu, A. Tukker, B. Steubing, Future material demand for automotive lithium-based batteries, Commun Mater 1 (2020), https://doi.org/10.1038/s43246-020-00095-x.
[21] J. Le Bideau, L. Viau, A. Vioux, Ionogels, ionic liquid based hybrid materials, Chem Soc Rev 40 (2011) 907–925, https://doi.org/10.1039/c0cs00059k.
[22] R. Sahrash, A. Siddiqa, H. Razzaq, T. Iqbal, S. Qaisar, PVDF based ionogels: applications towards electrochemical devices and membrane separation processes, Heliyon 4 (2018), https://doi.org/10.1016/j.heliyon.2018.e00847.
[23] L. Negre, B. Daffos, V. Turq, P.L. Taberna, P. Simon, Ionogel-based solid-state supercapacitor operating over a wide range of temperature, Electrochim Acta 206 (2016) 490–495, https://doi.org/10.1016/j.electacta.2016.02.013.
[24] P. Vallet, S. Bouzón-Capelo, T. Méndez-Morales, V. Gómez-González, Y. Arosa, R. de la Fuente, E. López-Lago, J.R. Rodríguez, L.J. Gallego, J.J. Parajó, J. Salgado, M. Turmine, L. Segade, O. Cabeza, L.M. Varela, On the physical properties of mixtures of nitrate salts and protic ionic liquids, J Mol Liq 350 (2022) 118483, https://doi.org/10.1016/j.molliq.2022.118483.
[25] X. Li, Q. Li, N. Lei, X. Chen, Luminescent sodium deoxycholate ionogel induced by Eu3+ in ethylammonium nitrate, ACS Omega 4 (2019) 2437–2444, https://doi.org/10.1021/acsomega.8b03555.
[26] A. Filippov, O.I. Gnezdilov, N. Hjalmarsson, O.N. Antzutkin, S. Glavatskih, I. Furó, M.W. Rutland, Acceleration of diffusion in ethylammonium nitrate ionic liquid confined between parallel glass plates, PCCP 19 (2017) 25853–25858, https://doi.org/10.1039/c7cp01772c.
[27] A. Filippov, O.N. Antzutkin, R. Gimatdinov, O.I. Gnezdilov, Self-diffusion in ionic liquids with nitrate anion: Effects of confinement between glass plates and static magnetic field, J Mol Liq 312 (2020), https://doi.org/10.1016/j.molliq.2020.113404.
[28] J. Salgado, J.J. Parajó, M. Villanueva, J.R. Rodríguez, O. Cabeza, L.M. Varela, Liquid range of ionic liquid – Metal salt mixtures for electrochemical applications, J Chem Thermodyn 134 (2019) 164–174, https://doi.org/10.1016/j.jct.2019.03.012.
[29] S.A.M. Noor, P.M. Bayley, M. Forsyth, D.R. MacFarlane, Ionogels based on ionic liquids as potential highly conductive solid state electrolytes, Electrochim Acta 91 (2013) 219–226, https://doi.org/10.1016/j.electacta.2012.11.113.
[30] E. Gómez, N. Calvar, Á. Domínguez, Thermal behaviour of pure Ionic Liquids, In: Scott Handy (Ed.), Ionic Liquids- Current State of the Art, INTECH, 2012: pp. 135–152. https://doi.org/10.5772/67458.
[31] M. Villanueva, J.J. Parajó, P.B. Sánchez, J. García, J. Salgado, Liquid range temperature of ionic liquids as potential working fluids for absorption heat pumps, J. Chem. Thermodyn. 91 (2015) 127–135, https://doi.org/10.1016/j.jct.2015.07.034.
[32] J. Salgado, J.J. Parajó, J. Fernández, M. Villanueva, Long-term thermal stability of some 1-butyl-1-methylpyrrolidinium ionic liquids, J. Chem. Thermodyn. 74 (2014) 51–57.
[33] T. Zentel, V. Overbeck, D. Michalik, O. Kühn, Hydrogen bonding in protic ionic liquids: structural correlations, vibrational spectroscopy, and rotational dynamics of liquid ethylammonium nitrate, J. Phys. B Atomic Mol. Phys. 51 (2018) 10.
[34] L.L. Hench, J.K. West, The Sol-Gel Process, Chem Rev 90 (1990) 33–72, https://doi.org/10.1021/cr00099a003.
[35] D. Ausín, J.J. Parajó, J.L. Trenzado, L.M. Varela, O. Cabeza, L. Segade, Influence of small quantities of water on the physical properties of alkylammonium nitrate ionic liquids, Int J Mol Sci 22 (2021), https://doi.org/10.3390/ijms22147334.
[36] A. Taubert, R. Löbbicke, B. Kirchner, F. Leroux, First examples of organosilica-based ionogels: Synthesis and electrochemical behavior, Beilstein Journal of Nanotechnology 8 (2017) 736–751, https://doi.org/10.3762/bjnano.8.77.
[37] A. Oleinikova, M. Bonetti, Critical behavior of the electrical conductivity of concentrated electrolytes: Ethylammonium nitrate in n-octanol binary mixture, J Solution Chem 31 (2002) 397–413, https://doi.org/10.1023/A:1015811432158.
[38] T.L. Greaves, A. Weerawardena, C. Fong, I. Krodkiewska, C.J. Drummond, Protic ionic liquids : Solvents with tunable phase behavior and physicochemical properties, J. Phys. Chem. B 110 (2006) 22479–22487, https://doi.org/10.1021/jp0634048.
[39] M. Galiński, A. Lewandowski, I. Stepniak, Ionic liquids as electrolytes, Electrochim Acta 51 (2006) 5567–5580, https://doi.org/10.1016/j.electacta.2006.03.016.
[40] D. Ausín, J.L. Trenzado, M. Turmine, L.M. Varela, O. Cabeza, E. González Romero, L. Segade, Influence of metal salts addition on physical and electrochemical properties of ethyl and propylammonium nitrate, Int J Mol Sci 23 (2022), https://doi.org/10.3390/ijms232416040.
[41] T. Vogl, S. Passerini, A. Balducci, The impact of mixtures of protic ionic liquids on the operative temperature range of use of battery systems, ElectrochemistyCommunications 78 (2017) 47–50, https://doi.org/10.1016/j.elecom.2013.11.010.
[42] K. Hayamizu, Y. Aihara, H. Nakagawa, T. Nukuda, W.S. Price, Ionic conduction and ion diffusion in binary room-temperature ionic liquids composed of [emim][BF4] and LiBF4, J. Phys. Chem. B 108 (2004) 19527–19532, https://doi.org/10.1021/jp0476601.
[43] A. Martinelli, A. Matic, P. Jacobsson, L. Börjesson, A. Fernicola, B. Scrosati, Phase behavior and ionic conductivity in LiTFSI doped ionic liquids of the pyrrolidinium cation and TFSI anion, J Phys Chem B 113 (2009) 11247–11251.
[44] J. Vila, E. Rilo, L. Segade, O. Cabeza, L.M. Varela, Electrical conductivity of aqueous solutions of aluminum salts, Phys Rev E Stat Nonlin Soft Matter Phys 71 (2005) 1–8, https://doi.org/10.1103/PhysRevE.71.031201.
[45] I.H. Sajid, M.F.M. Sabri, S.M. Said, M.F.M. Salleh, N.N.N. Ghazali, R. Saidur, B. Subramaniam, S.W. Hasan, H.A. Jaffery, Crosslinked thermoelectric hydro-ionogels: A new class of highly conductive thermoelectric materials, Energy Convers Manag 198 (2019), https://doi.org/10.1016/j.enconman.2019.111813.
[46] S. Bouzón- Capelo, T. Méndez-Morales, J. Carrete, E. López Lago, J. Vila, O. Cabeza, J.R. Rodríguez, M. Turmine, L.M. Varela, Effect of temperature and cationic chain length on the physical properties of ammonium nitrate-based protic ionic liquids, J. Phys. Chem. B 116 (2012) 11302–11312, https://doi.org/10.1021/jp3066822.
[47] J. Vila, P. Ginés, J.M. Pico, C. Franjo, E. Jiménez, L.M. Varela, O. Cabeza, Temperature dependence of the electrical conductivity in EMIM-based ionic liquids: Evidence of Vogel-Tamman-Fulcher behavior, Fluid Phase Equilib 242 (2006) 141–146, https://doi.org/10.1016/j.fluid.2006.01.022.
[48] J. Vila, P. Ginés, E. Rilo, O. Cabeza, L.M. Varela, Great increase of the electrical conductivity of ionic liquids in aqueous solutions, Fluid Phase Equilib 247 (2006) 32–39, https://doi.org/10.1016/j.fluid.2006.05.028.
[49] A. Guyomard-Lack, P.E. Delannoy, N. Dupré, C.V. Cerclier, B. Humbert, J. Le Bideau, Destructuring ionic liquids in ionogels: Enhanced fragility for solid devices, PCCP 16 (2014) 23639–23645, https://doi.org/10.1039/c4cp03187c.
[50] R.V. Pivato, F. Rossi, M. Ferro, F. Castiglione, F. Trotta, A. Mele, β-Cyclodextrin nanosponge hydrogels as drug delivery nanoarchitectonics for multistep drug release kinetics, ACS Appl Polym Mater 3 (2021) 6562–6571, https://doi.org/10.1021/acsapm.1c01262.
[51] T. Stettner, S. Gehrke, P. Ray, B. Kirchner, A. Balducci, Water in protic ionic liquids: Properties and use of a new class of electrolytes for energy-storage devices, ChemSusChem 12 (2019) 3827–3836, https://doi.org/10.1002/cssc.201901283.
[52] R. Zarrougui, M. Dhahbi, D. Lemordant, Transport and thermodynamic properties of ethylammonium nitrate – water binary mixtures : Effect of Temperature and Composition, J Solution Chem 44 (2015) 686–702, https://doi.org/10.1007/s10953-014-0283-z.
[53] M.E. Di Pietro, F. Castiglione, A. Mele, Polar/apolar domains' dynamics in alkylimidazolium ionic liquids unveiled by the dual receiver NMR 1H and 19F relaxation experiment, J Mol Liq 322 (2021) 114567, https://doi.org/10.1016/j.molliq.2020.114567.
[54] Y. Shimizu, Y. Wachi, K. Fujii, M. Imanari, K. Nishikawa, NMR Study on Ion Dynamics and Phase Behavior of a Piperidinium-Based Room-Temperature Ionic Liquid: 1-Butyl-1-methylpiperidinium Bis(fluorosulfonyl)amide, J. Phys. Chem. B 120 (2016) 5710–5719, https://doi.org/10.1021/acs.jpcb.6b04095.
[55] D. Bernin, D. Topgaard, NMR diffusion and relaxation correlation methods: New insights in heterogeneous materials, Curr Opin Colloid, Interface Sci 18 (2013) 166–172, https://doi.org/10.1016/j.cocis.2013.03.007.
[56] P. Galvosas, P.T. Callaghan, Multi-dimensional inverse Laplace spectroscopy in the NMR of porous media, C R Phys 11 (2010) 172–180, https://doi.org/10.1016/j.crhy.2010.06.014.